Closed Dynamic Soaring Trajectories for Surveillance Missions of Aerial Vehicles

David Emanuel de Castro Ventura Alexandre
david.v.alexandre@tecnico.ulisboa.pt

Instituto Superior Técnico, Universidade de Lisboa, Portugal
Università di Roma "La Sapienza", Rome, Italy

December 2019

Abstract

Dynamic soaring is a flight technique used by albatrosses to cover large distances without the expenditure of energy, which is extracted from the available wind conditions. Closed dynamic soaring trajectories use spatial variations of wind speed to hover, in principle, indefinitely over a prescribed area. Applying the concept of closed dynamic soaring trajectories to aerial vehicles, in particular, UAVs may provide a solution to improve the endurance of these vehicles in certain particular missions. The main limitation of dynamic soaring is its dependence on the wind. The present work studies the feasibility of closed, single-loop, energy-neutral trajectories for a broad set of conditions. Through the use of trajectory optimization methods, it was possible to see how the wind profile, initial flight conditions and vehicle constraints influence the required wind strength to perform dynamic soaring and consequently the trajectories' viability. It was possible to conclude from the study that there are optimal values for the initial airspeed and initial height of the vehicle, that minimise the required wind strength to perform the trajectories. In addition, it was seen that the structural and aerodynamic constraints of the vehicle affect dynamic soaring trajectories at high and low airspeeds respectively. The work ends by proposing some new trajectories that can be performed in conditions of excess wind to maximize the time spent on the air and the trajectory length while maintaining the concept of single-loop, energy-neutral trajectories, making them especially useful for aerial vehicles surveillance applications.

Keywords: trajectory optimization, non-linear flight dynamics, energy-harvesting, endurance, feasibility conditions

1. Introduction

Dynamic soaring is a flight technique in which a bird (or vehicle) takes advantage of the spatial wind variations, to maintain itself aloft. For dynamic soaring to occur, there must be an increase in wind speed with altitude. In these conditions, the vehicle can perform a dynamic soaring manoeuvre, consisting of a climb into the increasing wind, an upper turn, a descent with the wind and a lower turn to return to the original heading.

By performing dynamic soaring manoeuvres, the aerial vehicle can take advantage of the strong winds at high altitudes to gain energy, while using the comparatively weak winds at lower altitudes to minimize the losses [1].

Dynamic soaring manoeuvres are, in nature, used by the wandering albatross as a technique to cover vast distances without expenditure of energy. In aeronautical aplications, dynamic soaring has been used to break speed records of RC models with great success [2].

The concept of dynamic soaring was first introduced by Lord Rayleigh in 1883 through the observations of the flight of pelicans [3].

Through the years, many different authors contributed to the study of this phenomenon [4–7]. Most recently, in 2019 new papers have appeared, Sachs [2, 8, 9] presented new optimizations where he focuses on maximizing the net travel speed for different wind strengths, presented the case for how dynamic soaring is used for achieving record-breaking speeds for UAVs, and provided an in-depth description of the energy-harvesting mechanism of dynamic soaring. Kai [10] took a new approach to the modeling and simulation of dynamic soaring, estimating analytically the expressions for different variables associated with dynamic soaring, such as the minimum wind speed required.

Dynamic soaring is a promising solution for increasing endurance of mini and micro UAVs since,

to perform dynamic soaring manoeuvres, it is not necessary to extensively modify the vehicle, being only required to follow a pre-defined trajectory. In the future, this is expected to be calculated by the UAVs onboard computers.

The possibility of increasing the operational endurance of small fixed-wing UAVs would allow them to compete with their larger counterparts, while maintaining low operational costs and higher deployment flexibility.

The main drawback of dynamic soaring is the dependence on the environmental conditions around the vehicle. The specificity of the wind conditions required for dynamic soaring limits its applicability.

It is in the context of the limitations of the dynamic soaring mechanism that the present research will be conducted. The main goals of this work are to understand how the applicability of dynamic soaring manoeuvres is affected by different factors and propose trajectories optimised for surveillance missions.

2. Numerical Implementation

2.1. Equations of Motion

The equations of motion (EoM) for a UAV will be developed based on three preliminary assumptions [11]:

- The Earth is considered as flat and non-rotating;
- The UAV is assumed as particle, characterized by its centre of mass, thus all inertia terms related with rotation should be neglected;
- The wind blows steadily from the North.

To obtain the full picture of a UAV's motion, it is necessary to consider four different frames: the Earth frame ($O(\boldsymbol{e}_x^E, \boldsymbol{e}_y^E, \boldsymbol{e}_z^E)$) , the North-East-Down (NED) frame ($U(\boldsymbol{e}_x^{E'}, \boldsymbol{e}_y^{E'}, \boldsymbol{e}_z^{E'})$), the flight path frame ($U(\boldsymbol{e}_x^F, \boldsymbol{e}_y^F, \boldsymbol{e}_z^F)$) and the wind frame ($U(\boldsymbol{e}_x^W, \boldsymbol{e}_y^W, \boldsymbol{e}_z^W)$). Figure 1 presents the relationship between the various frames.

For the UAV model being developed, there are two types of forces that should be considered: the gravitational force and the aerodynamic force. Thrust forces will not be considered since the desired trajectories should be performed without the use of a propulsion system. These forces acting on the vehicle can then be written, respectively, as

$$\boldsymbol{F}_{\boldsymbol{G}}^E = mg\boldsymbol{e}_z^E, \tag{1}$$

where m is the UAV mass and g is the modulus of the gravitational acceleration, and

$$\boldsymbol{F}_{\boldsymbol{A}}^W = -D\boldsymbol{e}_x^W - L\boldsymbol{e}_z^W, \tag{2}$$

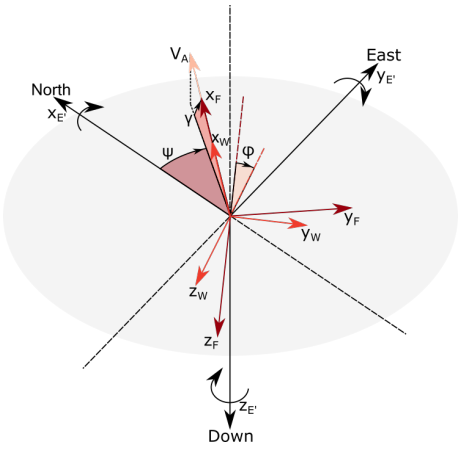

Figure 1: Relationship between the NED, Flight Path(in red) and Wind (in orange) frames. Earth frame not represented, it is parallel to the NED frame but centered in the ground. Adapted from [7]

with the intensity of the lift and drag, neglecting compressibility effects, calculated based on

$$L = \frac{1}{2}\rho S V_A^2 C_L, \tag{3}$$

$$D = \frac{1}{2}\rho S V_A^2 C_D, \tag{4}$$

$$C_D = C_{D_0} + K C_L^2, \tag{5}$$

where $V_A$is the vehicle's airspeed, ρ is the air density, S is the wing area, C_L is the lift coefficient, C_D is the drag coefficient, C_{D_0} is the viscous zero lift drag coefficient and K the induced drag coefficient.

In what concerns the modelling of the wind, different models can be applied to study the dynamic soaring phenomenon. The most common models are: the linear wind model,

$$\boldsymbol{W}^E = \beta h \boldsymbol{e}_x^E, \tag{6}$$

where h is the altitude of the UAV, being equivalent to the symmetric of the z coordinate of the Earth frame ($h = -z^E$), and β is the wind gradient slope; the logarithmic wind model,

$$\boldsymbol{W}^E = W_{ref}\frac{ln(h/h_0)}{ln(h_{ref}/h_0)}\boldsymbol{e}_x^E, \tag{7}$$

where h_{ref} its a reference altitude, h_0 is the wind profile starting altitude and W_{ref} is the wind speed at the reference altitude; and the step wind model,

$$\boldsymbol{W}^E = \frac{A}{2}(\tanh(k(h-b))+1)\boldsymbol{e}_x^E, \tag{8}$$

where A is the maximum wind speed, k controls the steepness of the gradient and b is the transition height, at which half of the step is reached.

With all previous considerations in mind, it is possible to write the set of equations of motion in the flight path frame,

$$\dot{V_A} = -\frac{1}{m}D - g\sin\gamma - \cos\gamma\cos\psi\dot{W}_x^E, \tag{9a}$$

$$V_A\cos\gamma\dot{\psi} = \frac{1}{m}L\sin\phi + \sin\psi\dot{W}_x^E, \tag{9b}$$

$$V_A\dot{\gamma} = \frac{1}{m}L\cos\phi - g\cos\gamma + \sin\gamma\cos\psi\dot{W}_x^E, \tag{9c}$$

$$\dot{x} = V_A\cos\gamma\cos\psi + W_x^E, \tag{9d}$$

$$\dot{y} = V_A\cos\gamma\sin\psi, \tag{9e}$$

$$\dot{z} = -V_A\sin\gamma. \tag{9f}$$

The study of the motion of the UAV needs to be accompanied by a study of the energy exchanges that occur during its motion. The rate of change of mechanical energy is equal to the power of non-conservative forces (NCF)

$$\frac{dE_m}{dt} = \sum(\boldsymbol{F_{NCF}^E}\cdot\boldsymbol{V_G^E}). \tag{10}$$

Since the only non-conservative forces present in this model are the lift and drag of the UAV, it is possible to split the rate of change of mechanical energy into a contribution due to lift, and one due to drag,

$$\frac{dE_m}{dt} = -LW_x^E(\cos\phi\sin\gamma\cos\psi + \sin\phi\sin\psi) - DV_A - DW_x^E\cos\gamma\cos\psi, \tag{11}$$

Looking at equation (11), it is possible to verify that the contribution of lift to the variation of mechanical energy depends directly on the wind. Thus, in no wind condition there can only be energy loss, since there is only the negative contribution of drag.

2.2. Trajectory Optimization

The study of dynamic soaring trajectories can be seen as a trajectory optimization problem in which it is desired minimize a given objective function such as the required wind speed.

In general, it was desired to minimize the required wind strength for dynamic soaring, while respecting the equations of motion of the vehicle, and ensuring that the initial and final positions of the vehicle are equal, as well as the airspeed. The result are closed, energy-neutral trajectories. In addition the trajectories were also forced to be single-loop by forcing that the final heading angle be 2π greater than the initial one. In addition, during the trajectory the vehicle cannot exceed a maximum load factor (n), representing its structural limitations and given by,

$$n = \frac{L}{W} = \frac{0.5\rho SV_A^2C_L}{mg} \leq 3. \tag{12}$$

The trajectory optimization problem can be solved using different techniques. Following the work of several authors [6–8, 12] a direct method will be used. The method has essentially, two phases: a transcription phase that converts the problem into a non linear program (NLP); and a solving phase, where a NLP solver applies an optimization algorithm to find the solution.

To transcribe the problem, it is necessary to descretize the continuous trajectory into a set of points in time, called collocation points, each one with a specific value for the state and control variables. So, if the UAV trajectory is discretized into N points in a time interval $[0, t_f]$, there are N time unknowns,

$$\boldsymbol{t} = t_0, ..., t_k, ..., t_N, \tag{13}$$

6N state unknowns, the x, y and z position coordinates of the vehicle, the airspeed V_A and the heading and flight path angles, ψ and γ,

$$\boldsymbol{x} = x_0^i, ..., x_k^i, ..., x_N^i, i = 1, 2, 3, 4, 5, 6, \tag{14}$$

and 2N control unknowns, the lift coefficient C_L and bank angle ϕ,

$$\boldsymbol{u} = u_0^j, ..., u_k^j, ..., u_N^j, j = 1, 2, \tag{15}$$

resulting in a total of 9N unknowns. This set of unknowns represents the set of variables that comprise the design vector $\boldsymbol{z}$. Note that after determining the initial and final time of the trajectory, all time unknowns can be calculated using the spacing between the collocation points.

With the trajectory discretized, it is also necessary to discretize the continuous system dynamics, represented by the differential equations. To discretize them, an integration rule is used, such as the trapezoidal rule. The numerical integration of the differential equations between two collocation points establishes a relationship between them. For a generic differential equation,

$$\dot{x^i} = f^i(\boldsymbol{x}(t), \boldsymbol{u}(t)), \tag{16}$$

the use of the trapezoidal rule establishes a relationship between two consecutive collocation points [8],

$$(x_{k+1}^i - x_k^i) - \frac{1}{2}(f_k^i + f_{k+1}^i)(t_{k+1} - t_k) = 0, \tag{17}$$

so for the 6 differential equations that comprise the UAV dynamics, there are a total of 6(N-1) equality constraints related to the system dynamics.

Other constraints are applied independently to each collocation point.

The NLP obtained from the transcription can be solved using a interior point method, which converts the constrained NLP into an unconstrained optimization method and then proceeds to use a

Newton method to solve the problem[13]. Interior point methods are specially designed to tackle this kind of problems, being robust and well documented methods.

In the developed work, the transcription was made using the Imperial College London Optimal Control Software (ICLOCS2) [14] and the NLP solver choosen was Interior Point Optimizer (IPOPT) [15].

3. Energy-Harvesting Mechanism

An in-depth analysis of the energy-harvesting mechanism associated with dynamic soaring must be done before presenting any other results since the discussion of any optimal trajectory requires understanding the underlying mechanism that allows for dynamic soaring to happen.

The aim is to understand how the different phases of the dynamic soaring trajectory contribute for the maintenance of the energy-neutral condition. Thus, since dynamic soaring may be of particular interest for applications of surveillance, the analysis of the energy-harvesting mechanism will be made considering a closed trajectory that minimizes the wind strength required for an energy-neutral loop, meaning that, at the end of the trajectory, the vehicle will have maintained its initial potential and kinetic energy. During its motion, the vehicle will be subject to a linear wind profile, chosen for its simplicity.

Figures 2 and 3 present the optimal trajectory obtained from the numerical procedure. The minimized slope obtained for the linear wind profile (β of eq. (6)), was $0.3s^{-1}$, which corresponds to a wind velocity of 6m/s at an altitude of 20m.

The solution was obtained using 300 collocation points and the open trajectory from the verification as the initial guess. The numerical tool required 217 iterations to obtain the final solution which corresponded to a computational time of 186s in a computer with a Intel® Core™ i7-8750H @ 2.20Hz processor.

3.1. Climb

During the climbing phase, altitude is gained in exchange for a loss in airspeed. Because the UAV is going into the wind, the ground speed is always lower than the airspeed, figure 3 shows just that. In addition, the flight path angle is positive ($\gamma > 0$), the heading angle is between $\frac{\pi}{2}$ and $\frac{3\pi}{2}$ since the UAV it is pointing in the southward direction (against the wind blowing north), and because it is a closed-loop trajectory, the UAV banks right ($\phi > 0$).

Looking at the energy contributions, also presented in figure 3 it is possible to verify that the lift contribution is positive and increases over time, as a result of the increasing wind speed.

To better understand how the lift can contribute

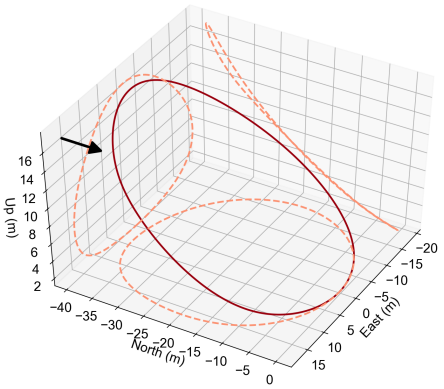

Figure 2: Optimal single-loop, energy-neutral trajectory that minimises the wind strength required in a linear wind profile. Arrow indicates the wind direction. The dashed lines represent the trajectory projections, on each of the three planes. The vehicle travels in the clock-wise direction.

positively to the overall energy of the system, it is helpful to consider a simplified case in which the climb occurs with wings leveled ($\phi = 0$) and with the UAV pointing directly southward ($\psi = \pi$). These assumption can be made without loss of generality. For the simplified case equation (11) becomes

$$\frac{dE_m}{dt} = LW_x^E \sin\gamma + DW_x^E \cos\gamma - DV_A, \quad (18)$$

and for a positive variation of the mechanical energy,

$$\frac{L}{D}\frac{W_x^E}{V_A}\sin\gamma + \frac{W_x^E}{V_A}\cos\gamma - 1 > 0, \quad (19)$$

which means that during the climb, the energy gain depends essentially on the wind strength and on the L/D ratio. Figure 4 presents a schematic of the forces acting of the UAV during the climb, where it is possible to see how a component of the lift vector acts in the direction of the ground speed, acting as a pseudo thrust force F, providing energy to the vehicle. The term pseudo comes from the fact that the component acts in the direction of the ground speed and not the airspeed.

The pseudo thrust force, only exists as a result of the existent wind velocity vector. In the case in which the wind strength is zero, the air velocity vector and ground velocity vector are the same, and lift is orthogonal to both, and does not provide energy to the system.

3.2. Upper-Turn

The next phase of the flight is the upper turn. During this phase the, UAV continues the turn to the right ($\phi > 0$) and goes from facing southward

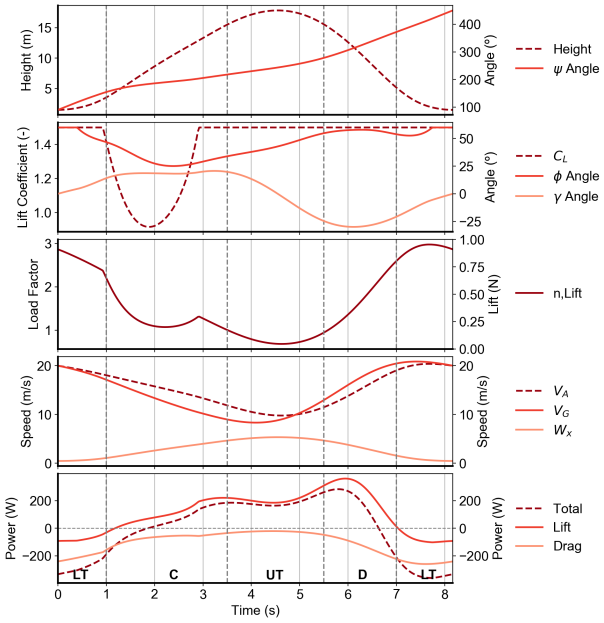

Figure 3: Detailed evolution of the principal parameters of the optimal trajectory that minimizes the wind strength required for a linear wind profile. The first panel presents the evolution of the altitude and heading angle with time. The second panel presents the evolution of the control variables and the flight path angle. The third panel presents the evolution of the lift and load factor with time (the lines are coincident). The fourth panel presents the evolution of the ground speed, airspeed and wind speed throughout the trajectory. Finally, the last panel presents the evolution of the lift and drag contributions for the variation of the mechanical energy, as well as the overall variation of the energy (LT - Lower Turn, C - Climb, UT - Upper Turn, D - Descent).

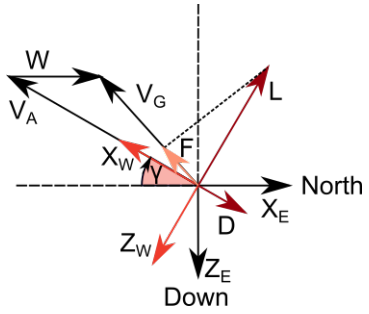

Figure 4: Diagram of the climbing phase in the vertical plane, for wing levelled conditions ($\phi = 0$) and pointing south ($\psi = \pi$) (See [9]).

to facing northward, so that it may, eventually, descend with the wind. In addition, the flight path angle goes from positive to negative in preparation for the descent. Also, during the upper turn, the UAV reaches its maximum altitude and minimum airspeed.

For the described conditions, and looking again at equation (11) and figure 3, it is possible to verify that the lift continues to provide energy to the UAV. The drag also continues to contribute to the energy variation negatively. The small drag contribution, $-DW_x^E \cos\gamma \cos\psi$ goes from attenuating the drag losses to also contribute negatively to the energy of the system, since the signal of $\cos\psi$ changes.

Figure 5 presents the schematic of the forces acting on the UAV in the upper turn, for the simplified case, where it is assumed the turn occurs in leveled flight ($\gamma = 0$). In this conditions, equation (11) becomes

$$\frac{dE_m}{dt} = -LW_x^E \sin\phi \sin\psi - DV_A - DW_x^E \cos\psi. \tag{20}$$

During a turn from $\psi = \pi$ to $\psi = 2\pi$, $\sin\psi < 0$ and $\sin\phi > 0$, resulting in a positive contribution from the lift throughout the turn.

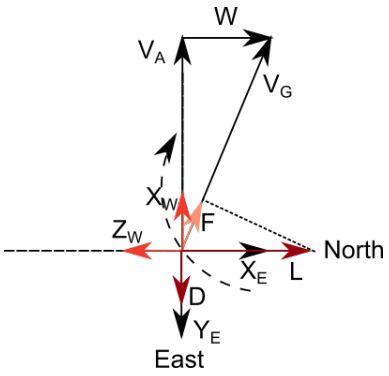

Figure 5: Diagram of forces, in the horizontal plane, for the middle of the upper turn ($\psi = 3\pi/2$) and for leveled flight ($\gamma = 0$) (See [9]).

3.3. Descent

The descent phase is characterized by a loss in altitude in exchange for a gain in airspeed. The ground speed is always higher than the airspeed because the UAV is descending with the wind.

For the case of the loop presented, the UAV continues to bank right ($\phi > 0$), while the flight path angle is negative ($\gamma < 0$) and the vehicle is pointing northward ($3\frac{\pi}{2} < \psi < 5\frac{\pi}{2}$).

Looking at the evolution of the energy contributions present in figure 3, it is possible to verify that the lift keeps providing a positive contribution to the energy of the system.

If the simplified case of descent without banking ($\phi = 0$) and facing directly north ($\psi = 0$) is considered, then equation (11) becomes

$$\frac{dE_m}{dt} = -LW_x^E \sin\gamma - DV_A - DW_x^E \cos\gamma \tag{21}$$

and, to insure a positive rate for the mechanical energy, the following condition must be respected,

$$-\frac{L}{D}\frac{W_x^E}{V_A}\sin\gamma - \frac{W_x^E}{V_A}\cos\gamma - 1 > 0. \tag{22}$$

It is then clear that the lift contribution is still positive and, just as in the climb, depends on the wind-strength and L/D ratio. Figure 6 presents the schematic representation of the simplified case of the descent.

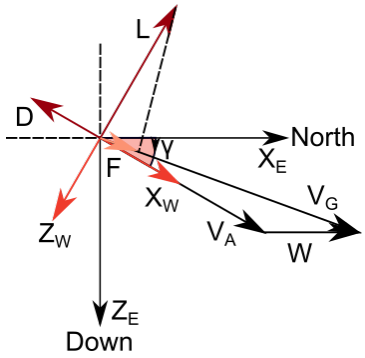

Figure 6: Diagram of forces, in the vertical plane, during the descent phase without banking ($\phi = 2\pi$) and pointing north ($\psi = 0$) (See [9]).

3.4. Lower Turn

Finally, the last phase of the flight is the lower turn. This turn will bring the UAV to its initial condition. This phase is characterized by being part of the flight where the energy losses of the system occur. Looking at figure 3, it is possible to verify that during this phase the rate of mechanical energy of the system is negative, and both the lift and drag contributions are negative.

During this phase, the UAV continues to bank right ($\phi > 0$), the flight path angle goes from negative to positive, and the UAV goes from pointing northward to southward in preparation for another loop. Equation (11) allows for the understanding of why the lift contributes negatively during this phase.

This negative contribution is better understood when considering the simplified case in which it is assumed that the turn occurs with flight path angle equal to zero ($\gamma = 0$), simplifying equation (11) ,

$$\frac{dE_m}{dt} = -LW_x^E \sin\phi\sin\psi - DV_A - DW_x^E\cos\psi.$$

Looking at the simplified equation it is possible to verify that, when wind is present, the lift contributes negatively, since $\sin\psi > 0$ in a turn from 2π to 3π. Figure 7 presents the schematization of this simplified flight phase, where F represents the component of the lift that now acts as an additional drag contribution.

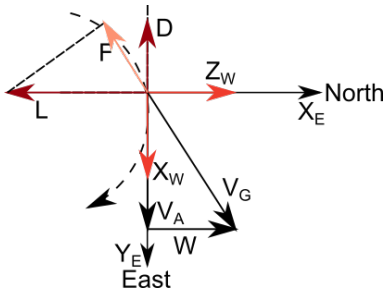

Figure 7: Diagram of forces, in the horizontal plane of the UAV, during the lower turn for $\gamma = 0$ and ($\psi = 5\pi/2$) (See [9]).

4. Feasibility of Dynamic Soaring

The objective now is to find how the wind profile, the initial conditions and vehicle constraints affect dynamic soaring trajectories and the viability of their execution. To perform this study, only closed, single-loop, energy-neutral dynamic soaring trajectories will be considered, since they represent manoeuvres that an aerial vehicle is expected to perform in a surveillance mission.

4.1. Comparison Metrics

To draw comparisons between the trajectories and to understand how the various factors affect their feasibility and performance, it is necessary to establish a set of metrics that can be used to compare them.

Since the focus of the research is to study the feasibility of dynamic soaring trajectories, it is useful to define metrics that consider trajectories that require high wind strengths as inefficient, since they have a higher dependence on the wind for energy extraction.

With the previous considerations in mind, the first quantity that can be used to perform comparisons is real wind speed delta,

$$\Delta W_r = W(h_{max}) - W(h_{min}), \tag{23}$$

where h_{max} and h_{min} are the highest and lowest altitudes attained by the UAV during the trajectory respectively. Since the wind gradient with altitude is always positive, it means that this metric compares the maximum and minimum wind speeds to which the vehicle is subjected.

Using the concept of real wind speed delta, two other quantities can be defined, a parameter based on the maximum height,

$$\eta_h = \frac{h_{max}}{\Delta W_r t_s}, \tag{24}$$

and a parameter based on the trajectory's length,

$$\eta_l = \frac{l}{\Delta W_r t_s}, \tag{25}$$

where, t_s is the time spent to perform the full trajectory and l is the total distance travelled. These two new quantities establish a relation between the wind speed required and the net speed of the trajectory, with the net speed being given by $\frac{h_{max}}{t_s}$ or by $\frac{l}{t_s}$.

4.2. Effect of the Wind Profile

Table 1 summarizes the main characteristics of the closed, energy-neutral trajectories that minimise the required wind strength, obtained for the different wind profiles. It also presents the respective values for the metrics previously presented.

Table 1: Comparison between dynamic soaring trajectories for different wind profiles, for a initial airspeed of 20m/s and an initial height of 1.5m.

Wind Profile	t_s [s]	h_{max} [m]	l [m]	ΔW_r [m/s]	η_h	η_l
Linear	8.16	17.85	119.26	4.88	0.45	2.99
Logarithmic	11.57	14.82	167.29	5.16	0.25	2.81
Step 1 (k=0.5 and b=5)	7.64	16.26	119.29	3.40	0.63	4.59
Step 2 (k=0.5 and b=10)	7.85	16.00	117.36	3.86	0.53	3.87
Step 3 (k=0.5 and b=15)	9.05	18.28	119.00	6.46	0.31	2.03
Step 4 (k=0.7 and b=5)	7.59	16.31	118.62	3.31	0.65	4.73
Step 5 (k=1.1 and b=5)	7.56	16.27	118.28	3.23	0.67	4.85

Looking at table 1, it is possible to conclude that the wind profiles that require the least amount of wind strength, for the given initial conditions, are the step wind profiles with transition height (b of equation (8)) equal to 5 and 10 meters. In contrast, the least efficient wind profile is the step wind profile with transition height equal to 15 meters, which requires almost double the wind strength when compared with the other step wind profiles. From table 1, it is also possible to conclude that by increasing the steepness k of the step-profile, there is a slight decrease in the required wind strength.

For the initial conditions considered, the linear and logarithmic wind profiles require a higher wind strength than the best step wind profiles, but lower than step 3. The trajectory obtained for the logarithmic wind profile requires the second-largest wind strength for the cases presented and results in a trajectory larger than for any other case.

From table 1 it is also possible to verify that, in general, as the required wind strength increases, the time and length of the trajectory also increase.

The reason behind the fact that the trajectory for the step 3 wind profile requires more wind speed than the remainder step profiles is because the vehicle is forced to climb during much more time without the presence of wind, or in other words, without being capable of extracting energy. When it reaches the 15-meter altitude, its airspeed is very small, and consequently, there is a reduction in lift available to provide energy, when compared with the other two cases. The result is that to extract the same amount of energy, the only possibility is to have stronger winds.

The difference between steps 1 and 2 is not as significant because lift depends on the square of the airspeed. So as the airspeed decreases, the energy-extraction decreases with the square of the airspeed difference, which needs to be compensated with increasing wind speed. Since the trajectory for b=15 implies flying with lower airspeeds than for the other two cases, the impact of the transition height becomes more notorious.

The decrease in the required wind with increased steepness can be explained from the fact that in the lower turn, there is an increasing negative lift contribution with decreasing wind steepness. This negative contribution is the result of the presence of wind that, as the steepness decreases, increases in intensity. This analysis allows for the conclusion that the presence of wind speed in the lower turn reduces the efficiency of the trajectory.

4.3. Effect of the Initial Conditions

All results presented until now considered the same set of initial conditions. From the previous discussion, it seems reasonable to assume that, by changing the initial conditions of the vehicle, the efficiency attributed to each wind profile may change. If the conditions are not the most suitable, then the vehicle cannot extract the highest amount of energy from the profile and the feasibility of the trajectory may be compromised.

Initial Height

Figure 8 presents the evolution of the required wind strength as function of the initial height for the case of the step 2 wind profile.

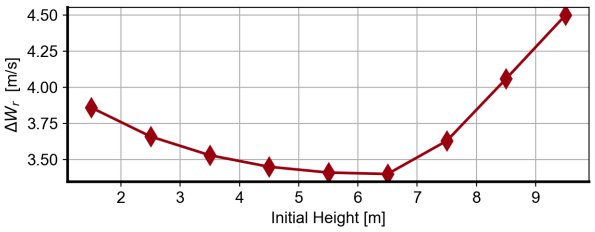

Figure 8: Evolution of the required wind speed as a function of the initial height for a step-wind profile with b=10 and k=0.5.

Looking at the figure, it is possible to verify that there is an initial height that minimizes the wind strength required. The optimal altitude is around 6.5 meters. This behaviour is the result of two phenomena. Firstly, when the initial height is lower than the optimal value, the vehicle is forced to climb and descend without extracting energy during most of the time. Secondly, if the initial height is increased beyond the optimal value, it means that the lower turn will occur in the presence of higher

wind speeds, which increases the losses of the vehicle. From figure 8, it is also possible to conclude that, from the two phenomena, it is the presence of wind speed in the lower turn, that most negatively contributes to loss of efficiency and, consequently, a loss of viability.

Initial Airspeed

Figure 9 presents the evolution of the real wind speed delta as a function of the initial airspeed, for the case of step 1, 2 and 3, all with k = 0.5 and for each of the transition heights.

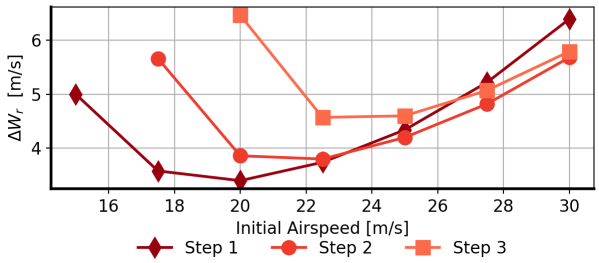

Figure 9: Evolution of the required wind strength as a function of the initial airspeed for three different step-wind profiles with b=5,10 and 15, and k=0.5.

Analysing figure 9, it is possible to see that there also is an initial airspeed that minimises the required wind speed. In addition, it is possible to verify that, depending on the initial airspeed, the most efficient step-wind profile changes. As expected, the step with the lowest transition height is the most efficient profile for low airspeeds, while the profiles with higher transitions heights are better for higher initial airspeeds.

A couple of factors can explain the behaviour verified for the four cases presented. At lower than optimal initial airspeeds, the increase of the required wind speed is the result of a decrease in the capacity of the vehicle to extract energy. The lift depends on the square of the airspeed so at lower airspeeds the contribution of the lift for the energy is reduced. In addition, for step-wind profiles with high transition heights, there are not feasible trajectories for low initial airspeeds since the vehicle does not have sufficient initial airspeed to trade in order to reach the transition height.

On the other side, at higher than optimal initial airspeeds, the increase of the minimum wind speed can be explained based on two factors. On the one hand, although the energy extraction increases with the airspeed, so does the drag, resulting in a need of higher wind speeds. On the other hand, the limitation imposed by the maximum load factor admissible, limits the maximum airspeed and turn rate of the vehicle can reach, resulting in less efficient trajectories.

4.4. Effect of Vehicle Constraints

From the previous discussion regarding the variation of performance with initial airspeed, it was possible to verify that the maximum lift coefficient and maximum load factor influence the feasibility of dynamic soaring manoeuvres. Figure 10 presents the evolution of the required wind strength as a function of the initial airspeed, for different vehicle constraints and considering the case of the step 2 wind profile.

From this analysis, it is possible to verify that when the C_L maximum is low, it is the C_L that limits the feasibility and performance of the trajectories. On the contrary, when C_L maximum is high, then it is the load factor that limits the feasibility and performance that can be extracted. Moreover, depending on the initial airspeed, one factor may be of higher importance than the other.

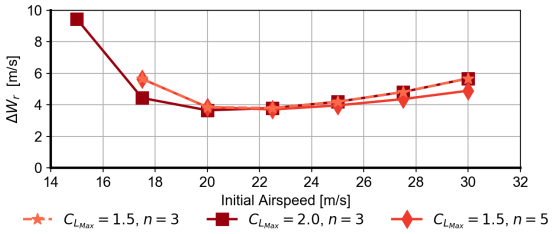

Figure 10: Evolution of the required wind strength as a function of the initial airspeed, for different vehicle constraints.

Looking again at figure 10, it is possible to verify that, on the one hand, at lower initial airspeeds, it is possible to obtain more efficient trajectories (trajectories that require less wind strength) by having a larger value of the maximum lift coefficient, while at higher airspeeds the maximum lift coefficient does not contribute to any changes. On the other hand, by having a larger maximum load factor it is possible to obtain more efficient trajectories,at higher initial airspeeds, while at lower airspeeds it does not change the performance. The reason behind this phenomenon is the fact that the load factor is the main constraint at higher airspeeds, while at lower airspeeds it is the lift coefficient.

In addition, it is possible to verify that the maximum lift coefficient and the maximum load factor change the feasibility region. For instance, for an initial airspeed of 15m/s and a step-wind profile with transition height at 10 meters, there is not a feasible trajectory when the maximum lift coefficient is 1.5. In contrast, if the maximum lift coefficient is 2.0, then it is possible to find a feasible trajectory.

5. Surveillance Trajectories

Until now, the trajectories considered were obtained with the objective of minimising the necessary wind speed to perform them. The question now is what can be done when the wind strength is higher than the minimum required.

The aim is to find trajectories that, utilising favourable wind conditions, can be used for surveillance missions. Thus, the obtained trajectories must be closed, single-loop and energy-neutral, in order to have trajectories with simple control schemes (the UAV can only bank to one side), and that are endlessly repeatable in constant wind conditions.

Since the interest is on developing trajectories for surveillance missions, there are two characteristics of the trajectory that should be optimized: the trajectory time and length.

Figures 11 and 12 present the trajectory that maximizes the flight time of the closed, single-loop, energy-neutral trajectory for a step-wind profile with b=5 and k=0.5, and with a maximum wind strength (A of eq. (8)), equal to 5m/s.

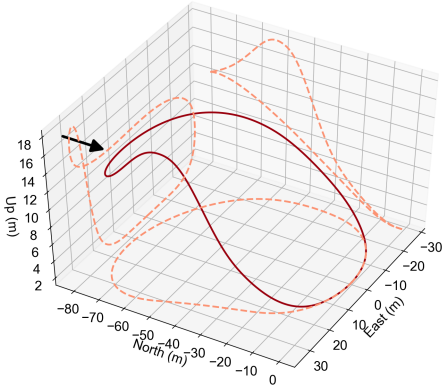

Figure 11: Optimal single-loop, energy-neutral trajectory that maximizes the time aloft. Arrow indicates the wind direction. The vehicle travels in the clock-wise direction.

Looking at figures 11 and , it is possible to verify that the behaviour of the vehicle during the manoeuvre has changed when compared with the previous cases studied. The trajectory obtained is still a simple single-loop closed trajectory, but after the initial climb, there is a small descent into the wind, that generates a loss of energy. Afterwards, the upper turn occurs at almost constant height, followed by the descent and the lower turn.

The new behaviour for the trajectory can be explained by the fact that, to have an energy-neutral trajectory in excess wind conditions, it is necessary to waste the additional energy gained due to the stronger wind speed. Since the objective is to increase the flight time, the solution is to waste the

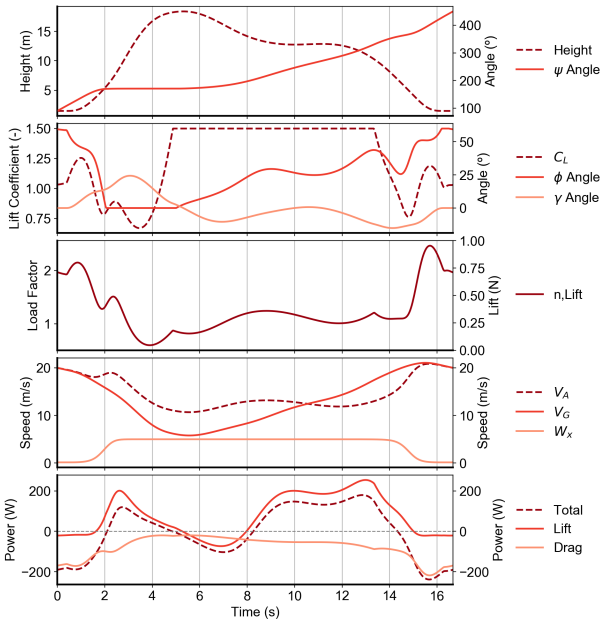

Figure 12: Detailed evolution of the principal parameters of the optimal trajectory Evolution of the trajectory that maximizes flight time for a surveillance mission.

excess energy in a way that the trajectory time increases. The small descent into the wind, combined with the longer upper turn, allows for such overall.

6. Conclusions

In the present research, it was possible to analyse the dynamic soaring phenomenon from different perspectives. From the study of the energy-harvesting mechanism of dynamic soaring, it was possible to conclude that two variables condition the energy-harvesting: the lift-drag ratio and the existent wind speed. In addition, it was also possible to conclude that the need for a wind profile with a positive gradient in the height direction is due to the fact that, to perform dynamic soaring manoeuvres, it is necessary to have a maximisation of the energy extraction on the top of the trajectory and a minimisation of the losses on the lower part. This analysis complemented the research done by other authors.

The feasibility of dynamic soaring trajectories was also analysed. It was seen that factors such as initial airspeed and height change the required minimum wind speed for dynamic soaring, in different wind models. It was possible to conclude that there are optimal values for the initial conditions of the vehicle that minimise the required wind strength. In addition, it was possible to obtain curves that establish the division between the infeasible region and the excess wind energy region were also obtained. Finally, it was also possible to

conclude that the aerodynamic and structural limits of the vehicle, in the form of the maximum lift coefficient and load factor, influence the feasibility region of dynamic soaring, and that, in general, one of these two factors will limit the performance of the dynamic soaring trajectory.

Finally, the present research was able to develop trajectories specially designed for surveillance missions. When excess wind conditions exist, it is possible to utilise the excess energy to extend the time aloft or the length of the trajectory.

References

[1] G. P. Sachs. Minimum shear wind strength required for dynamic soaring of albatrosses. *Ibis*, 147(1):1–10, Dec 2004. doi: 10.1111/j.1474-919x.2004.00295.x.

[2] G. P. Sachs. Dynamic soaring at 600 mph. *AIAA Scitech 2019 Forum, San Diego, USA*, Jan 2019. doi: 10.2514/6.2019-0107.

[3] Rayleigh. The soaring of birds. *Nature*, 27 (701):534–535, 1883. doi: 10.1038/027534a0.

[4] C. D. Cone. *A mathematical analysis of the dynamic soaring flight of the albatross with ecological interpretations*. Virginia Institute of Marine Science, 1964.

[5] C. J. Pennycuick. Soaring behaviour and performance of some east african birds, observed from a motor-glider. *Ibis*, 114 (2):178–218, 1971. doi: 10.1111/j.1474-919x.1972.tb02603.x.

[6] G. C. Bower. *Boundary Layer Dynamic Soaring for Autonomous Aircraft: Design and Validation*. PhD thesis, Stanford University, USA, 2012.

[7] V. Bonnin, C. Toomer, J.-M. Moschetta, and E. Benard. Energy harvesting mechanisms for UAV flight by dynamic soaring. *International Journal of Micro Air Vehicles*, 7(3):213–230, 2015. doi: 10.2514/6.2013-4841.

[8] G. P. Sachs and B. Grüter. Maximum travel speed performance of albatrosses and UAVs using dynamic soaring. *AIAA Scitech 2019 Forum, San Diego, USA*, Jan 2019. doi: 10.2514/6.2019-0568.

[9] G. P. Sachs. Kinetic energy in dynamic soaring - inertial speed and airspeed. *Journal of Guidance, and Dynamics*, 42(8):1812–1821, Jun 2019. doi: 10.2514/1.G003407.

[10] J.-M. Kai, T. Hamel, and C. Samson. Novel approach to dynamic soaring modeling and simulation. *Journal of Guidance, Control, and Dynamics*, 42(6):1250–1260, 2019. doi: 10.2514/1.g003866.

[11] I. Mir, S. A. Eisa, and A. Maqsood. Review of dynamic soaring: technical aspects, nonlinear modeling perspectives and future directions. *Nonlinear Dynamics*, 94(4):3117–3144, 2018. doi: 10.1007/s11071-018-4540-3.

[12] Y. J. Zhao. Optimal patterns of glider dynamic soaring. *Optimal Control Applications and Methods*, 25(2):67–89, 2004. doi: 10.1002/oca.739.

[13] A. C. Marta. Aircraft optimal design. MSc Course Notes, 2019, Insituto Superior Técnico, Lisboa, Portugal.

[14] Y. Nie, O. Faqir, and E. Kerrigan. ICLOCS2: A MATLAB toolbox for optimization based control. URL `http://www.ee.ic.ac.uk/ICLOCS/default.htm`. [Online. Accessed 5th October 2019].

[15] A. Wächter and L. T. Biegler. On the implementation of an interior-point filter line-search algorithm for large-scale nonlinear programming. *Mathematical Programming*, 106(1): 25–57, 2005. doi: 10.1007/s10107-004-0559-y.